Simultaneous determination of dissolved inorganic carbon (DIC) concentration and stable isotope (δ^{13}C-DIC) by Cavity Ring-Down Spectroscopy: Application to study carbonate dynamics in the Chesapeake Bay

Jianzhong Su[a,b], Wei-Jun Cai[a*], Najid Hussain[a], Jean Brodeur[a], Baoshan Chen[a], and Kuan Huang[c]

[a]School of Marine Science and Policy, University of Delaware, Newark, DE 19716, USA

[b]State Key Laboratory of Marine Environmental Science, Xiamen University, Xiamen, 361005, China

[c]Picarro Inc., CA 950504, USA

Correspondence to Wei-Jun Cai, wcai@udel.edu

Abstract

Dissolved inorganic carbon (DIC) and its stable isotope (δ^{13}C-DIC) are powerful tools for exploring aquatic biogeochemistry and the carbon cycle. Traditionally, they are determined separately with a DIC analyzer and an isotope ratio mass spectrometer. We present an approach that uses a whole-water CO_2 extraction device coupled to a Cavity Ring-Down Spectroscopy (CRDS) CO_2 and isotopic analyzer to measure DIC and δ^{13}C-DIC simultaneously in a 3-4 mL sample over an ~11 min interval, with an average precision of 1.5±0.6 μmol kg^{-1} for DIC and 0.09±0.05 ‰ for δ^{13}C-DIC. The system was tested on samples collected from a Chesapeake Bay cruise in May 2016, achieving a precision of 0.7±0.5 μmol kg^{-1} for DIC and 0.05±0.02 ‰ for δ^{13}C-DIC. Using the simultaneously measured DIC and δ^{13}C-DIC data, the biogeochemical controls on DIC and its isotope composition in the bay during spring are discussed. In the northern upper

bay, the main controlling processes were CO_2 outgassing and carbonate precipitation, whereas primary production (surface) and degradation of organic carbon (subsurface) dominated in the southern upper bay and middle bay. By improving the mode of sample introduction, the system could be automated to measure multiple samples. This would give the system the potential to provide continuous shipboard measurements during field surveys, making this method more powerful for exploring the complicated carbonate system across a wide range of aquatic settings.

Keywords

Dissolved inorganic carbon; stable carbon isotope; Cavity Ring-Down Spectroscopy; Chesapeake Bay; estuarine carbon cycle

1. Introduction

Dissolved inorganic carbon (DIC) is the sum of all dissolved forms of inorganic carbon including aqueous carbon dioxide (CO_{2aq}), carbonic acid (H_2CO_3), bicarbonate (HCO_3^-) and carbonate (CO_3^{2-}), and it is the major pool of carbon in most natural waters (Zeebe and Wolf-Gladrow, 2001; Bianchi, 2011a). Its stable isotope abundance is expressed as per mil deviations from the reference standard Vienna-PeeDee Belemnite (V-PDB) and denoted as $\delta^{13}C$ in ‰:

$$\delta^{13}\mathrm{C} = \left(\frac{\left({}^{13}C/{}^{12}C\right)_{sample}}{\left({}^{13}C/{}^{12}C\right)_{V-PDB}} - 1\right) \times 1000$$

Both DIC and $\delta^{13}C$-DIC are influenced by multiple physical and biogeochemical processes, such as mixing between river water and seawater, biological production, degradation of organic matter, formation or dissolution of calcium carbonate ($CaCO_3$),

and air-sea CO_2 exchange (Samanta et al., 2015). The deviations of DIC and δ^{13}C-DIC from conservative mixing can be regarded as fingerprints left by different biogeochemical processes. Therefore, together with other parameters such as salinity, nutrient concentrations and total alkalinity, DIC and δ^{13}C-DIC can be used as powerful tools in studies seeking to understand the sources and cycling processes of carbon in estuarine and coastal environments (Hellings et al., 1999; Hu et al., 2016; Wang et al., 2016; Su et al., 2017; Yang et al., 2018).

In estuarine and coastal research, discrete samples are typically taken to determine DIC and δ^{13}C-DIC separately. DIC can be measured through CO_2 extraction followed by different detection methodologies to quantify the released CO_2, including coulometry (Dickson et al., 2007; Amornthammarong et al., 2014), spectrophotometry (Wang et al., 2007), mass spectrometry (Cardenas-Valencia et al., 2013), isotope dilution (Huang et al., 2013; Huang et al., 2015), and non-dispersive infrared absorption (NDIR) (O'Sullivan and Millero, 1998). The NDIR method has a precision of 0.1 % or ±2 μmol kg^{-1} for seawater analysis (Friederich et al., 2002; Huang et al., 2012), and it is used in the method comparison performed in this analysis.

δ^{13}C-DIC is conventionally measured by isotope ratio mass spectrometry (IRMS) with precision better than 0.1 ‰ (Humphreys et al., 2015). So far, several optical spectroscopy techniques have been developed in order to overcome the expense and laboriousness of IRMS measurement, such as tunable diode laser absorption spectroscopy (TDLAS) (Bergamaschi et al., 1994), NDIR (Jäger et al., 2005), Fourier transform infrared spectroscopy (FTIR) (Mohn et al., 2007), and cavity enhanced or cavity ring-down methods (Jost et al., 2006; Wahl et al., 2006). Several attempts have been made to

69 determine DIC and δ^{13}C-DIC simultaneously by Cavity Ring-Down Spectrometer
70 (CRDS). For instance, Bass et al. (2012) used an acidification interface to extract CO_2
71 from a 350 mL sample in a chamber through ePTFE tubing, and determined the δ^{13}C of
72 the circulated CO_2 between the CRDS and the chamber at a 15 min interval, with a
73 precision of ±10 μmol kg^{-1} for DIC and ±0.2 ‰ for δ^{13}C-DIC. However, this method
74 requires a large sample volume, and the measurement uncertainty of DIC is larger than
75 the accepted practice of ±2 μmol kg^{-1}. Call et al. (2017) coupled two commercial
76 instruments, an Autonomous Infra-Red Inorganic Carbon Analyser (AIRICA) and a
77 CRDS, to measure DIC and δ^{13}C-DIC in sequence over a 16 min cycle on a sample
78 volume of 2 mL. They achieved a precision of 1.5-2 μmol kg^{-1} for DIC by AIRICA and
79 0.14±0.04 ‰ for δ^{13}C-DIC by CRDS at DIC > 1000 μmol kg^{-1}. Although their study
80 reduced the required sample volume to several milliliters without compromising isotope
81 precision, they had to utilize two analyzers (one NDIR and one CRDS) separately rather
82 than a single CRDS to determine both the DIC concentration and the isotope value. No
83 information about CRDS performance for DIC measurement was provided in their paper.
84 Huang et al. (2013, 2015) used isotope dilution methods to examine the capability of
85 CRDS for DIC analysis and achieved a high precision of <0.02 % in the laboratory and
86 <0.03 % in the field survey. While highly precise, this method uses two CRDS detectors
87 (one for δ^{13}C and one for δD and δ^{18}O as a flow tracer) and therefore is expensive and
88 not easy to set up for many users. The motivation of this study is to achieve simultaneous
89 determination of DIC and δ^{13}C-DIC with one CRDS detector and a small sample volume
90 to achieve high precision comparable with the traditional methods based on NDIR and
91 IRMS.

92 In our approach, a CO_2 extraction device and CRDS detector were coupled to
93 simultaneously measure DIC and $\delta^{13}C$ in a 3-4 mL sample over an ~11 min interval, with
94 average precision of 1.5±0.6 μmol kg^{-1} for DIC and 0.09±0.05 ‰ for $\delta^{13}C$-DIC. Note that
95 the average precision is calculated as the mean of uncertainties for each set of triplicate
96 measurements. Intercomparisons with conventional NDIR and IRMS methods were
97 performed to assess the precision and accuracy, injection volume effect, instrument
98 stability, and differences among three calibration methods. Furthermore, the efficacy of
99 this approach was examined by measuring samples collected from a Chesapeake Bay
100 cruise in May 2016, which resulted in a precision of 0.7±0.5 μmol kg^{-1} for DIC and
101 0.05±0.02 ‰ for $\delta^{13}C$-DIC. Finally, we analyzed the field dataset and provided
102 interpretations for the deviations of DIC and $\delta^{13}C$-DIC relative to conservative mixing,
103 which provides an example of applying this technique to distinguish the main
104 biogeochemical processes controlling DIC and its isotope composition in estuarine and
105 coastal ocean research.
106
107 **2. Materials and procedures**
108 **2.1 Instrumentation principles**
109 This system is essentially composed of a whole-water CO_2 extraction device and a
110 CRDS isotopic analyzer (G2131-i, Picarro, www.picarro.com) (Fig. 1). The CO_2
111 extraction device consists of a digital syringe pump (5.0 mL, Kloehn) for transferring
112 accurate amounts of reagent and sample, a highly efficient gas stripping reactor, and a
113 mass-flow-controller (Model #GFC17, Aalborg) to control the carrier gas flow precisely.
114 This device also uses a Nafion tube to reduce the water vapor. A pump with 4-port valve

was used for single-sample analysis in the present study, however recently the device has been upgraded with a 12-port valve designing for multi-sample analysis and become commercially available (AS-D1, Apollo Scitech, www.apolloscitech.com). The isotopic analyzer is based on a CRDS technique. A gas sample is introduced into a high-finesse optical cavity and the unique infrared absorption spectrums of trace gas species are determined, thus providing the concentration or isotopic ratio measurements of a particular gas species of interest, such as CO_2, H_2O and CH_4 (Crosson, 2008). More detailed principles and the performance evaluation of the CRDS instruments can be found elsewhere (Friedrichs et al., 2010; Nara et al., 2012). A single software routine is written for both units to operate CO_2 extraction procedures, read data and calculate results. For each measurement, an aliquot of sample is acidified in the gas stripper, CO_2 is extracted by the carrier gas, and the gas stream flows through a moisture condenser before measurement by CRDS. The software mentioned above can also acquire raw data from CRDS, integrate the CO_2 mixing ratio signal (Eq. (1)), and average the $\delta^{13}C$-CO_2 values (Eq. (2)). CO_2-free compressed air (UN1002, Keen Compressed Gas Co.) was used as a carrier gas to avoid the gas matrix effects on CO_2 and $\delta^{13}C$-CO_2, as demonstrated by Friedrichs et al. (2010). A vent is used to avoid pressure build-up at the inlet of the CRDS.

2.2 Procedure

The analytical procedure consists of the following steps:

Step 1: Establish baseline. At the beginning, CO_2-free carrier gas flows through the gas stripper and lowers the CO_2 value of the CRDS measurement down to 1-2 ppm.

Step 2: CO_2 stripping. The syringe pump first draws 1.5 mL phosphoric acid (5 % (vol./vol.) H_3PO_4 with 10 % (wt./vol.) NaCl), and injects 0.6 mL into the reactor for gas

stripping to get rid of the contaminant CO_2. Then, the pump draws a 3.8 mL sample on top of the remaining 0.9 mL acid in the syringe, and finally injects all liquid into the reactor for gas stripping, where dispensed carrier gas continues moving upward from the bottom to the top of the reactor (Fig. 1). DIC is thoroughly converted to CO_2, which is extracted by the carrier gas and flows through a condenser to reduce water vapor before measurement by CRDS.

Step 3: CO_2 detection. The CO_2 gas flows through the cavity and is detected by CRDS. Meanwhile, the raw data for CO_2 ($^{12}CO_2$+$^{13}CO_2$) and δ^{13}C-CO_2 are read from CRDS and are recorded at ~ 1 HZ frequency for a period of ~350 s. When the change of CO_2 measurements drops below a preset threshold (i.e., standard deviation of CO_2 for 15 consecutive data points is less than 0.15 ppm), the software will terminate the analysis, because there is only a small amount of CO_2 left in the reactor and further gas stripping would change the area integration value of CO_2 very slowly. Terminating the analysis at this point results in an uncertainty of duplicate analysis less than 0.1 %.

Step 4: Discharge. After measurement termination, the acidified sample is discharged and the system is flushed by CO_2-free carrier gas to return to near-blank condition. Then, the system is ready to run the next measurement cycle. The average time for each cycle is ~ 11 min.

2.3 Determination of DIC and δ^{13}C-DIC

Following the Apollo Scitech DIC analysis method, the software has a function to integrate the area under the CO_2 curve minus the area under a baseline to measure the concentration of DIC. A typical output from CRDS is shown in Fig. 2, in which CO_2 is stable and low (< 2 ppm) for the first 50 s, then sharply increases to a peak value, and

161 decreases to a low value (< 10 ppm) again. The start and end points for DIC integration
162 are set to values where standard deviation of CO_2 for 15 consecutive data points is less
163 than 0.15 ppm. The start and end points and their corresponding CO_2 values are used to
164 derive a baseline in order to eliminate the background effect on area integration. The net
165 area is integrated by the equation:

166 $$\text{Net Area} = \sum(CO_{2i}^{meas} - CO_{2i}^{base}) \times \Delta T_i \quad (1)$$

167 where CO_{2i}^{meas} represents the measured CO_2 value from CRDS at the *i*th measurement
168 interval, CO_{2i}^{base} represents the baseline value of CO_2 on the solid line in Fig. 2 at the
169 same interval, and ΔT_i is the time between the two consecutive intervals i+1 and i.

170 Meanwhile, the δ^{13}C-CO_2 signal is noisy and randomly distributed when CO_2 is low
171 (e.g., when CO_2 <100 ppm, standard deviation of δ^{13}C-CO_2 is ±42.1 ‰), but becomes
172 relatively stable when CO_2 is high (e.g. when CO_2 >100 (380) ppm, standard deviation of
173 δ^{13}C-CO_2 is ±0.99 (0.70) ‰). The manufacturer states that CRDS has a precision of 0.05 %
174 for CO_2 and 0.12 ‰ for δ^{13}C-CO_2 when the CO_2 concentration ranges from 380 to 2000
175 ppm, but the measurement uncertainty becomes larger as CO_2 decreases to less than 380
176 ppm. Thus, a cutoff value of CO_2 was set in order to decrease the influence of the less
177 accurate isotope data points at low CO_2. Above the CO_2 cutoff value, δ^{13}C-CO_2 is
178 relatively stable and suitable for averaging isotope data. The integrated net area above the
179 cutoff line is used as a weight for isotope averaging. The δ^{13}C-DIC is thus derived from
180 the following equation:

181 $$\delta^{13}C\text{-}DIC = \frac{\sum(CO_{2j}^{meas} - CO_2^{cutoff}) \times \Delta T_j \times \delta^{13}C\text{-}CO_{2j}}{\sum(CO_{2j}^{meas} - CO_2^{cutoff}) \times \Delta T_j} \quad (2)$$

where CO_2^{cutoff} represents the cutoff value of CO_2, CO_{2j}^{meas} is the measured CO_2 value at *j*th measurement interval, and $\delta^{13}C\text{-}CO_{2j}$ is the measured δ^{13}C-CO_2 value from CRDS at the same interval. Since the purpose of using a cutoff value is to define a period when δ^{13}C-CO_2 is relatively stable, the lower end (i.e., 380 ppm) of the suitable range recommended by the manufacturer (380-2000 ppm) is ideally suitable for the cutoff value. But in our case the cutoff value was arbitrarily set to 100 ppm, because the final results of δ^{13}C-DIC from one measurement were not significantly different (e.g., -0.16, -0.15, -0.16, -0.15, -0.15 and -0.16 ‰, respectively) when using different cutoff values of 100, 150, 200, 250, 300 and 380 ppm. This is largely because the detected CO_2 quickly increases beyond 380 ppm, so that the amount of data between 100 and 380 ppm is small relative to the total, which therefore has almost no influence on the final results of δ^{13}C-DIC. Adopting a low cutoff value of 100 ppm may have the advantage of allowing the method to be applicable to low DIC freshwater samples though further evaluation is needed.

2.4 Evaluation of system performance

As shown in Fig. 3, three sets of standards were employed for concentration and isotope calibrations. The DIC standard is the Dickson certified reference material (CRM; Batch 172, DIC = 2038.99 μmol kg^{-1}, Salinity = 33.450 psu) run at three different volumes (e.g., 2.0, 2.6 and 3.3 mL) to bracket the net area of unknown samples for calibration of DIC concentration. Since the curve integration approach measures the total amount of released CO_2, this approach uses three volumes of one CRM to create a three-point standard curve. This is the principle used in all Apollo Scitech DIC analyzers and its validity has been confirmed in our work by comparison using three concentrations at a single volume (e.g., 3.3 mL).

205 The isotope standards include an isotopically heavy standard STD1 (-2.74±0.10 ‰)
206 and a depleted standard STD2 (-19.17±0.10 ‰), which were made by dissolving
207 $NaHCO_3$ solids (LC229431, LabChem for STD1; S-233, Fisher Scientific for STD2) in
208 ultra-pure water (Milli-Q), and were verified by IRMS in the stable isotope facility,
209 University of California, Davis. The third standard SGL2 was also made by dissolving
210 $NaHCO_3$ solids in ultra-pure water (Milli-Q) but bubbling with air overnight, which was
211 then verified by NDIR for DIC concentration (2086.4 μmol kg^{-1}) and by IRMS for δ^{13}C-
212 DIC (-2.20±0.10 ‰). SGL2 was measured using three different volumes for calibrations
213 of both concentration and isotope. A series of prepared solutions with distinct DIC and
214 δ^{13}C-DIC values was made by diluting mixtures of two kinds of concentrated $NaHCO_3$
215 solutions, which have the same DIC concentration but different δ^{13}C-DIC values. The
216 prepared solutions have DIC ranging from ~750 to ~2100 μmol kg^{-1}, and δ^{13}C-DIC
217 ranging from -2.4 to -19.4 ‰. In addition, 4 L aged seawater (DIC = 2181.7 μmol kg^{-1},
218 $\delta^{13}C$ = -2.0 ‰) from the Gulf of Mexico (GOM) was stored in a gas-tight aluminum bag
219 for examining the repeatability and long-term stability of the instrument.
220 The three sets of standards were measured before and after each batch of samples,
221 which included prepared solutions and aged GOM seawater. Precision was evaluated
222 based on the standard deviations of at least three replicate determinations for each sample.
223 Accuracy was examined by comparing the DIC values between NDIR and CRDS
224 methods, and the δ^{13}C-DIC values between IRMS and CRDS methods using the prepared
225 solutions, aged GOM seawater and CRM. To test the instrument's stability, the results
226 calibrated by each day's working curves were compared with the first day's working
227 curve over a period of 83 h. Also, the effect of injection volume on DIC and δ^{13}C-DIC

228 was evaluated by running GOM seawater in 13 different injection volumes. Three
229 calibration methods were examined to correct the raw data from prepared solutions and
230 aged GOM seawater, including i) using CRM in three different volumes to calibrate DIC,
231 and using two isotopic standards STD1 and STD2 to calibrate δ^{13}C-DIC; ii) using SLG2
232 in three different volumes to calibrate both DIC and δ^{13}C-DIC (i.e., three-point
233 calibration for DIC and single-point calibration for δ^{13}C-DIC); and iii) using SLG2 in a
234 middle volume to calibrate both DIC and δ^{13}C-DIC (i.e., single-point calibration for both
235 DIC and δ^{13}C-DIC).

236 **2.5 Field work in the Chesapeake Bay**

237 The Chesapeake Bay is the largest estuary in the United States. The Bay is about 300
238 km long, with a relatively deep (20 to 30 m) but narrow (1 to 4 km) central channel
239 confined by a sill in its lower bay (Kemp et al., 2005). Broad shallow areas flank the
240 central channel throughout the bay (Boicourt et al., 1999). A three-day cruise was
241 conducted in early May, 2016 to test the performance of the system (Fig. 4). On 4-5 May
242 2016, we cruised from the upper bay (CB2.1) southwards to the middle bay (CB4.4). On
243 6 May, we started sampling at CB5.5 in the lower bay, and went northward to CB5.1.
244 Waters were pumped up to the deck for sampling from 3-5 depths at each station.
245 Salinities were measured in discrete samples using a Cole-Parmer® salinity meter (±0.1
246 psu). The deionized water and the Dickson CRM were used to calibrate salinity. A water
247 sample was preserved in a 250 mL borosilicate glass bottle with 50 μL saturated $HgCl_2$
248 solution for DIC and δ^{13}C-DIC analysis (Huang et al., 2012). About 4-5 mL sample was
249 first analyzed for DIC concentration using an AS-C3 DIC analyzer (Apollo Scitech),
250 which uses an NDIR-based detector (LI-7000, Li-Cor) (Huang et al., 2012). In the NDIR-

based analysis, 3-volume standardization (that is using 0.5, 0.7 and 0.9 mL of CRM Batch 150) was performed twice daily, one in the early morning and one in the late afternoon with one single CRM volume (0.7 mL) inserted in the mid-day as unknown to check the instrument stability. An analytical precision better than ±0.1 % was achieved each day.

The remaining sample was measured by CRDS for both DIC and δ^{13}C-DIC within 3 weeks. Since the analysis of field samples were performed before we thoroughly evaluated the different calibration methods, only a CRM (Batch 150, DIC = 2017.88 μmol kg^{-1}, Salinity = 33.343 psu) and a $NaHCO_3$ solution with known δ^{13}C-DIC (-1.95±0.02 ‰, n=3) were used as standards for calibrations of DIC concentration and isotope, respectively. The injection volumes for all standards and samples were set as 3.8 mL. Single-point calibrations were applied to both DIC and δ^{13}C-DIC of the field samples. Before isotopic analysis, the samples were stored in a cold room.

3. Results and discussion

3.1 Assessment of precision and accuracy

For the prepared solutions and aged GOM seawater measurement (n=87), the overall analytical uncertainty of DIC was 1.5±0.6 μmol kg^{-1} and of δ^{13}C-DIC was 0.09±0.05 ‰. The uncertainty in δ^{13}C-DIC did not increase when DIC decreased from ~2200 to ~750 μmol kg^{-1}. This is consistent with Bass et al. (2012), in which the standard deviation of δ^{13}C-DIC kept at < 0.2 ‰ at DIC above 360 μmol kg^{-1}.

The accuracy of DIC and δ^{13}C-DIC analysis was examined through direct comparison of CRDS with NDIR and IRMS measurements on the prepared solutions, aged GOM

274 seawater and CRM (Fig. 5). The average offset in measured DIC and δ^{13}C-DIC between
275 methods (i.e., DIC_CRDS - DIC_NDIR, and δ^{13}C-DIC_CRDS - δ^{13}C-DIC_IRMS) was -
276 0.7±3.1 μmol kg^{-1}, which is close to the uncertainty of the NDIR-based DIC
277 measurement (0.1 % or ±2 μmol kg^{-1}), and 0.13±0.12 ‰, which is close to the accuracy
278 of the IRMS measurement on δ^{13}C-DIC (0.1 ‰).
279 The assessment of precision and accuracy is consistent with a recently published paper
280 on a worldwide seawater δ^{13}C-DIC intercomparison exercise (Cheng et al., 2019).
281 Identical replicate samples (CRM Batch 157 and deep ocean seawater) were sent to 16
282 laboratories for analysis using methods of IRMS (14 groups), CRDS (1 group), and both
283 IRMS and Isotope Ratio Infrared Spectrometer (IRIS) (1 group). Among the 16
284 laboratories, Lab #9 utilized a similar apparatus (Apollo Scitech AS-D3 DIC analyzer
285 and Picarro G2201-i CRDS detector). This work achieves a within-lab precision of
286 ±0.12 ‰, and their average (uncorrected) deep ocean seawater results are within 0.01‰
287 relative to the all-lab average that was determined largely using IRMS (Cheng et al.,
288 2019). Therefore, the system used in the present study can simultaneously determine DIC
289 and δ^{13}C-DIC, achieving good precision and accuracy comparable to the established
290 analysis methods for typical coastal and oceanic waters. When compared with the
291 prevalent IRMS isotope measurements, this system has an additional advantage of getting
292 precise DIC analysis, because the traditional IRMS method does not provide precise
293 determination of DIC concentration as illustrated in an earlier interlaboratory comparison
294 study (van Geldern et al., 2013).

295 **3.2 Effect of Injection volumes on DIC and δ^{13}C-DIC**

296 The sample injection volume can be adjusted in the software for different types of
297 sampling sources, e.g., using a smaller injection volume for a high DIC sediment
298 porewater sample, and using a larger injection volume for a low DIC river water sample.
299 Therefore, a known aged GOM seawater sample (DIC_NDIR= 2181.7±2.6 μmol kg^{-1} and
300 δ^{13}C-DIC_IRMS= -2.24±0.10 ‰) was run in a series of injection volumes to see if
301 changes to the injection volume could affect the measurements of DIC and δ^{13}C-DIC
302 using the CRDS system (Fig. 3 and 6). As shown in Fig. 6, the average DIC_CRDS value
303 of aged GOM seawater with different injection volumes was 2180.7±2.0 μmol kg^{-1},
304 which is close to the DIC_NDIR value of 2181.7±2.6 μmol kg^{-1}. This suggests that
305 injection volume has virtually no effect on DIC in CRDS analysis. By contrast, δ^{13}C-
306 DIC_CRDS was stable (-2.04±0.06 ‰) with larger injection volumes (2.4 to 4.0 mL), but
307 became a little heavier (-1.84±0.08 ‰) when the injection volume was less than 2.4 mL.
308 This may be related to the fact that when the cutoff value was fixed at 100 ppm CO_2, the
309 smaller injection volume (< 2.4 mL) would produce a lower CO_2 peak and a smaller data
310 pool of δ^{13}C-CO_2 above 100 ppm. Thus, the weight of the less accurate and heavier δ^{13}C-
311 CO_2 (at 100-380 ppm CO_2 interval) may slightly increase and make the final δ^{13}C-DIC a
312 little heavier (Eq. (2)). Although a larger injection volume may increase the analysis
313 duration for each run, it can help to maintain a better repeatability of δ^{13}C-DIC. Note that
314 the injection volumes for the assessment of precision and accuracy (Section 3.1) are
315 larger than 2.4 mL. Also the overall δ^{13}C-DIC_CRDS of GOM seawater is about 0.2 ‰
316 heavier than the IRMS verified value (-2.24±0.10 ‰) (Fig. 6), which may be caused by
317 the invasion of isotopically lighter atmospheric CO_2 to the IRMS samples during the

transfer of GOM seawater from the air-tight aluminum bag into 250 mL borosilicate glass bottles (Call et al., 2017).

3.3 Instrument stability

Standard materials were measured in three rounds during an 83-hour determination of prepared solutions and GOM seawater. The instrument stability was examined by using the DIC offset of GOM seawater between the calibration that used the first day's working curve (May 22) and the calibration that used each day's working curves (May 22-24) (Fig. 7). The average offset value is 1.3±0.7 μmol kg^{-1}, which is within the measurement uncertainty, meaning there was almost no instrument drift for DIC. Meanwhile, the standard deviations of raw δ^{13}C-DIC for STD1 (0.08 ‰, n=9), STD2 (0.08 ‰, n=9) and aged GOM seawater with injection volume >2.4 mL (0.06 ‰, n=55) were within the measurement uncertainty, indicating there was also no significant drift for the isotope measurement. High instrument stability shows the potential for autonomous and long-term measurement of DIC and δ^{13}C-DIC with infrequent calibrations in field surveys at sea.

3.4 Comparison of different calibration methods

Three different calibration methods were compared in our lab evaluation to see if single-point calibration could substitute for regular calibrations for DIC (three-point calibration) and δ^{13}C-DIC (two-point calibration) in daily operation, so as to i) decrease the time cost spent on running reference materials and increase the sample measurement efficiency; and ii) establish a correction relationship between single-point and regular calibrations. The first method used CRM in three different sample volumes to bracket the net integration area of samples for DIC calibration and two IRMS-verified isotopic

341 standards STD1 and STD2 to calibrate the δ^{13}C-DIC. This approach is similar to the
342 calibrations of DIC in NDIR and of δ^{13}C-DIC in IRMS. The second method used one
343 standard SGL2, whose DIC and δ^{13}C-DIC have been verified on NDIR and IRMS, also in
344 three different sample volumes. Thus, SGL2 could produce a working curve of carbon
345 content (μmol C) vs. net area bracketing all the samples for DIC calibration, and one
346 known isotopic value to calibrate δ^{13}C-DIC. For the third method, the data of middle
347 sample volume of SGL2 was chosen to calibrate DIC and δ^{13}C-DIC so as to minimize the
348 calibration time.
349 As shown in Fig. 8a, the first two methods had similar results for DIC offset relative to
350 NDIR, while the third method had a more positive offset at DIC < 1200 μmol kg^{-1}, but
351 more negative offset at DIC > 1400 μmol kg^{-1}. This is because the assumption behind
352 single-point calibration for DIC, that is, a unit net integration area represents a constant
353 carbon content, is not true in this case. There was an increasing trend for carbon content
354 per unit net area at low net area < 120000, but it remained constant thereafter (Fig. 9).
355 The net integration area of the prepared solutions and aged GOM seawater ranged from
356 50505 to 10366, existing on the increasing zone. As the middle volume of SGL2 in the
357 third method with net area of 89541±73 and 6.04×10^{-5} μmol C per unit net area was
358 adopted for calibration, the DIC of prepared solutions and aged GOM seawater with net
359 area < 89541 were overestimated, and > 89541 were underestimated. The over- or under-
360 estimates are within ±4 μmol kg^{-1} compared with the first and second methods. When
361 considering the relationship between net area and carbon content per unit net integration
362 area of SGL2 in three different volumes (Fig. 9), we can recalibrate the SGL2 middle
363 volume calibration data and get similar results as the first and second methods (Fig. 8a).

As for δ^{13}C-DIC, the first method uses a linear regression of measured and true δ^{13}C-DIC values of two laboratory reference standards, i.e., STD1 and STD2, to normalize the measured δ^{13}C of unknown samples to the true δ^{13}C in the isotope reference scale (Paul et al., 2007). The two-point normalization method has been proven to efficiently evaluate the consistency of δ^{13}C measurements in interlaboratory comparison work (Coplen et al., 2006), and it has been implemented in the Laboratory Information Management System distributed by the United States Geological Survey (Paul et al., 2007). The offset between the first calibration method and IRMS values is 0.13±0.12 ‰, approaching the analytical precision of isotopic measurements. The second and third calibration methods are single-point normalizations referencing a laboratory isotopic standard SGL2 (-2.20±0.10 ‰), using the measured and true values of the reference standard to calibrate the measured values of samples. Their offset relative to δ^{13}C-DIC_IRMS systematically increased from 0.08 to 0.62 ‰ as the absolute δ^{13}C-DIC difference between samples and reference standard increased from 0.04 to 17.43 ‰ (Fig. 8b). Paul et al. (2007) mathematically demonstrated this kind of systematic error associated with single-point anchoring. Overall, we suggest that three different CRM volumes be used to calibrate DIC concentration, and two different isotopic standards be used to calibrate δ^{13}C-DIC value, ensuring that the ranges of net area and isotope content of samples are covered by the standards.

3.5 DIC and δ^{13}C-DIC in the Chesapeake Bay

For the field samples, the DIC values measured by CRDS had an average precision of 0.7±0.5 μmol kg^{-1}, and agreed well with those measured by NDIR (DIC_NDIR=0.9921×DIC_CRDS+12.727, R^2=0.9999). The average offset between

measured DIC_CRDS and DIC_NDIR was only -0.6±3.8 μmol kg^{-1}, which is close to that of the lab test. The δ^{13}C-DIC values of the field samples determined by CRDS had an average precision of 0.05±0.02 ‰, but were not verified by IRMS. However, according to the relationship between single-point calibrated δ^{13}C-DIC_CRDS and IRMS measured δ^{13}C-DIC (i.e., δ^{13}C-DIC_IRMS) in Fig. 8b (grey), the average offset between methods was -0.12±0.05 ‰, which is also close to that of the lab test. Further corrections were not made to the single-point calibrated DIC_CRDS and δ^{13}C-DIC_CRDS because their average offset between methods were close to the precision and accuracy of measurements. As salinity increased, DIC increased from 951.2 μmol kg^{-1} at the uppermost station CB2.1 to 1894.6 μmol kg^{-1} in deep water in the middle bay (Fig. 10). Meanwhile, δ^{13}C-DIC increased from -7.68 ‰ near the freshwater zone to -0.73 ‰ in the surface water of CB5.5. Generally, DIC was lower and δ^{13}C-DIC was heavier in the surface water of the middle bay, while DIC became enriched and δ^{13}C-DIC became more depleted as depth increased.

3.6 Two-endmember mixing model

In estuaries and coastal environments, physical mixing between freshwater and seawater usually dominates the distribution of DIC and δ^{13}C-DIC. These parameters are also altered by different biogeochemical processes such as air-water CO_2 exchange, biological production and organic matter degradation (Alling et al., 2012; Samanta et al., 2015). In this study, we aimed to remove the effect of physical mixing and focus on the biogeochemical processes by using the DIC and δ^{13}C-DIC data. A two-endmember mixing model between the Susquehanna River endmember at Conowingo Dam and the offshore seawater endmember in the Mid-Atlantic Bight was adopted to predict the

conservative values of DIC and δ^{13}C-DIC driven by physical mixing in the Chesapeake Bay.

Using salinity as a conservative tracer, the mixing fractions between river water and seawater for each sample can be quantified using equations (3) and (4):

$$f_R + f_{SW} = 1 \quad (3)$$

$$S_R \times f_R + S_{SW} \times f_{SW} = S_{meas} \quad (4)$$

S represents salinity; *f* is the mixing fraction; the subscripts *R* and *SW* denote the River and Seawater endmember, and *meas* represents the measured value. These fractions were applied to predict conservative DIC and δ^{13}C-DIC resulting solely from two-endmember mixing:

$$DIC_{mix} = DIC_R \times f_R + DIC_{SW} \times f_{SW} \quad (5)$$

$$\delta^{13}C\text{-}DIC_{mix} = \frac{\delta^{13}C\text{-}DIC_R \times DIC_R \times f_R + \delta^{13}C\text{-}DIC_{SW} \times DIC_{SW} \times f_{SW}}{DIC_{mix}} \quad (6)$$

Subscript *mix* means conservative mixing value.

For the riverine DIC endmember, we compiled the historical DIC data measured by Cai's lab during August 2015-April 2017 (n=35) with the daily discharge rate Q from USGS (Site number 01578310), and then obtained linear relationships of DIC vs. LogQ (DIC= -540*LogQ+2714, R^2=0.49, p<0.0001). Considering the relatively long residence time of ~180 days in the Chesapeake Bay (Du and Shen, 2016), the specific discharge rate during the cruise period and 30 days prior was used to derive the riverine DIC endmember value (i.e., 1091.7±73.6 μmol kg^{-1}). Although the discharge varied ~20 % during the cruise period and multiple periods (10, 20, 30, 50, 70 and 90 d) prior to the cruise, it had only a small influence on the derived riverine DIC endmember values (< 5 %), within the uncertainty listed in Table 1. Hossler and Bauer (2012) monitored the

433 carbon isotopes of DIC in eight rivers in the U.S. east coast, including the Susquehanna
434 River, at approximately 3-4 month intervals during 2005-2007, and observed a general
435 pattern of summer-depleted and winter-enriched δ^{13}C-DIC signatures. The average value
436 of δ^{13}C-DIC in the spring and summer of 2006 was adopted as the riverine δ^{13}C-DIC
437 endmember value (-7.3±0.2 ‰). For the offshore DIC endmember, a linear regression of
438 DIC vs. salinity (DIC=79.1*Sal-596.5, R^2=0.72) was derived with data from four stations
439 (Sta. 82, 83, 85 and 87) in the Mid-Atlantic Bight, which were visited in the East Coast
440 Ocean Acidification (ECOA) cruise in July 2015. Then, the salinity of the ocean
441 endmember (33.618±0.139 psu) in Cai et al. (2017) was used to derive the offshore DIC
442 endmember value (2063.5±11.0 μmol kg^{-1}). Quay et al. (2007) compiled data from 28
443 cruises since 1986 to summarize the meridional trends of δ^{13}C-DIC in the surface
444 Atlantic Ocean in three time domains, the 1980s, 1990s and 2000s. According to the
445 latitude range of the Chesapeake Bay (36-40 °N), the offshore δ^{13}C-DIC endmember
446 value was adopted as 1.3±0.1 ‰. Both the offshore seawater DIC and δ^{13}C-DIC
447 endmember values fall into the ranges in the Mid-Atlantic Bight reported by Bauer et al.
448 (2001).

449 **3.7 Main biogeochemical controls on DIC composition in the Chesapeake Bay**

450 Using the river and offshore endmember values determined above, conservative
451 mixing lines for DIC and for δ^{13}C-DIC against salinity were established (Fig. 10). A
452 significant number of DIC and δ^{13}C-DIC data points were distributed above or beneath
453 the conservative mixing lines, indicating that other processes played an important role in
454 DIC and its isotope distributions in the Chesapeake Bay (Fig. 10). Since the processes
455 that change DIC may have distinct δ^{13}C source values and isotopic fractionation, it is

advantageous to use both DIC and δ^{13}C-DIC to distinguish them. Using a method similar to Alling et al. (2012) and Samanta et al. (2015), the fractional deviations of DIC (ΔDIC) and δ^{13}C-DIC ($\Delta\delta^{13}$C-DIC) relative to the conservative mixing values were calculated according to the following equations.

$$\Delta DIC = \frac{DIC_{meas} - DIC_{mix}}{DIC_{mix}} \quad (3)$$

$$\Delta\delta^{13}C\text{-}DIC = \delta^{13}C\text{-}DIC_{meas} - \delta^{13}C\text{-}DIC_{mix} \quad (4)$$

The propagation errors of ΔDIC and $\Delta\delta^{13}$C-DIC for each sample were calculated based on Taylor's expression (Taylor, 1997; Han et al., 2012).

As shown in Fig. 11 ($\Delta\delta^{13}$C-DIC vs. ΔDIC), the data can be explained as the combined result of five processes: CO_2 outgassing, biological production, degradation of organic carbon, carbonate precipitation and carbonate dissolution. The different vectors for the five processes were calculated according to the approach and equations given in Samanta et al. (2015). There are four likely vectors for the degradation of organic carbon, depending on the initial DIC and δ^{13}C-DIC composition in the water and the sources of organic carbon. Combining the δ^{13}C values of organic carbon from terrestrial (-28.0 ‰) and marine (-21.0 ‰) sources with the δ^{13}C-DIC endmember values in river water (-7.3 ‰) and offshore seawater (1.3 ‰), the slopes of these vectors were calculated as -20.7 (on river water or vector TR) and -29.3 (on seawater or vector TS) for degradation of terrestrial organic carbon, and -13.7 (on river water or vector MR) and -22.3 (on seawater or vector MS) for degradation of marine organic carbon. Assuming the δ^{13}C of biogenic $CaCO_3$ is 0 ‰, the slopes for carbonate dissolution were calculated as 7.3 in the low salinity zone (vector DR) and -1.3 in the high salinity zone (vector DS). As carbonate precipitation is the reverse of dissolution, the slopes of vectors for carbonate

precipitation will be -7.3 and 1.3 (vectors PR & PS). Using the average temperature (13.4 ℃) of the surface water in this cruise, the equilibrium fractionation factor between aqueous CO_2 and HCO_3^- were calculated as -10.2 ‰ (Rau et al., 1996). Therefore, the slope value of vector for CO_2 outgassing is -10.2. Assuming the phytoplankton preferentially utilize aqueous CO_2 as a carbon source, the photosynthesis activity would have two stages of isotopic fractionation when DIC is transferred into POC (Alling et al., 2012). In the first stage, there is a temperature-dependent equilibrium fractionation factor between δ^{13}C-DIC (approximately equal to δ^{13}C-HCO_3^-) and aqueous CO_2, which was -10.2 ‰ as mentioned before. In the second stage, the aqueous CO_2, which is equilibrated with the atmospheric CO_2 (δ^{13}C-CO_2 = -8 ‰) (Gruber et al., 1999), is incorporated into POC with an average δ^{13}C-POC value of -23.8 ‰ (W-J. Cai unpublished data), resulting in a fractionation factor of -15.8 ‰. Thus, the total isotope fractionation between δ^{13}C-DIC and δ^{13}C-POC is calculated as -26.0 ‰ by summing up the fractionation factors in the two stages. Therefore, the slope of the vector for primary production is -26.0.

All data from stations CB2.1 and 2.2 in the northern part of upper bay lie on the third quadrant (Fig. 11), which can be explained by carbonate precipitation alone or seen as the combined results of carbonate precipitation and CO_2 outgassing. When moving southward to the southern part of the upper bay and the middle bay, most of the data in the surface water fall on the second quadrant, indicating that CO_2 outgassing and/or CO_2 removal via biological production are the main processes controlling the DIC and δ^{13}C-DIC of surface water. In contrast, the majority of data in the bottom water lie on the fourth quadrant, meaning that the DIC and δ^{13}C-DIC of the bottom water in the southern part of upper bay and the middle bay are primarily controlled by degradation of organic

502 carbon. Data from the intermediate depths are distributed between the surface and bottom
503 data, which is understandable as water is a continuum for mixing of dissolved chemical
504 species.
505 These results are consistent with previous investigations (Kemp et al., 1997; Cai et al.,
506 2017). For instance, Kemp et al. (1997) estimated the net ecosystem metabolism of three
507 regions in the Chesapeake Bay along the land-sea gradient, and concluded that
508 community respiration exceeded primary production in the upper bay, which was caused
509 by the combined effects of allochthonous organic carbon input and high turbidity
510 conditions that enhanced respiration and inhibited photosynthesis (Smith and Kemp,
511 1995). Cai et al. (2017) measured supersaturated pCO_2 and undersaturated O_2 in the
512 northern regions of the bay, confirming that the CO_2 outgassing process prevailed in the
513 upper bay surface water. Su et al. (2018, in preparation) found that the submerged aquatic
514 vegetation (SAV) beds in the shallow regions along the bay, such as SAVs in the
515 Susquehanna Flats, can work as biogenic $CaCO_3$ factories to produce $CaCO_3$ solids on a
516 local scale. Thus, carbonate precipitation and CO_2 outgassing control the distribution of
517 DIC and $\delta^{13}C$-DIC in the northern part of the upper bay. In contrast to net heterotrophy in
518 the upper bay, the integrated metabolism in the middle bay is nearly balanced and net
519 autotrophy dominates in the lower bay (Kemp et al., 1997). Given the two-layer structure
520 in the water column in the middle bay in May (Schubel and Pritchard, 1986), the
521 carbonate and oxygen vertical dynamics would be distinct, with pCO_2 undersaturated and
522 oxygen supersaturated in the surface water and an increasing DIC enrichment and oxygen
523 deficit as depth increases in the water below the pycnocline. The underway pCO_2
524 measurement in this cruise showed that the surface water in the middle bay is a weak sink

525 of atmospheric CO_2 (W-J. Cai unpublished data), which is consistent with previous
526 published work (Cai et al., 2017). In the bottom water of the middle bay, oxygen is
527 seasonally depleted due to the deep channel topography, water stratification and supply
528 of labile autochthonous organic matter. Oxygen-based estimates of metabolism have
529 demonstrated that bottom-layer net O_2 consumption rates were highly correlated with
530 surface-layer net O_2 production rates (Smith and Kemp, 1995). Although Cai et al. (2017)
531 concluded that carbonate dissolution can contribute up to 70 % of the total amount of TA
532 production in the middle bay in August 2013, few data points fell in the first quadrant,
533 indicating that carbonate dissolution was not a major controlling process for DIC and
534 δ^{13}C-DIC in the water column in early May, 2016. However, it is possible that some
535 $CaCO_3$ dissolution may shift the bottom data points from near vector MS to closer to
536 vector MR (Fig. 11). Further study is needed to resolve this issue. Long-term dissolved
537 oxygen data have revealed that hypoxia occurs in the Chesapeake Bay from early June
538 through September in almost every year with large biweekly variability (Murphy et al.,
539 2011). Considering the average winter-spring (January to May) Susquehanna River flow
540 in 2016 was 20 % below the 50-year average (1967 to 2017), the onset timing of
541 hypoxia/anoxia in the main channel would probably have occurred later than early June
542 (Hagy et al., 2004). This is further confirmed by another cruise conducted during 6-10
543 June 2016, in which hydrogen sulfide was not detected in the main channel (W-J. Cai
544 unpublished data). For our cruise in early May, it was too early to develop a severe and
545 large hypoxic/anoxic zone in the bottom water of middle bay, which is consistent with a
546 much weaker signal of carbonate dissolution relative to August. Therefore, DIC and

547 δ^{13}C-DIC in the middle bay were primarily controlled by biological production and
548 degradation of organic carbon in early May, 2016.
549
550 **4. Conclusions**
551 Our study demonstrates that simultaneous measurement of DIC and δ^{13}C-DIC by
552 coupling a CO_2 extraction device and CRDS can generate highly accurate and precise
553 data, comparable to the traditional methods of NDIR for DIC analysis and IRMS for
554 δ^{13}C-DIC analysis. Consequently, this approach provides efficient and economical
555 measurements of these two parameters with a single instrument. Other advantages
556 include the small sample volume requirement (3-4 mL), short measurement cycle (~11
557 min.), and easy handling. To date, the paired DIC and δ^{13}C-DIC dataset remains limited
558 (Quay et al., 2003; Becker et al., 2012; Becker et al., 2016). Much more effort is needed
559 to expand the temporal and spatial coverage of this database. By adding an automatic
560 sampling module or changing the 4-port to 12-port distribution valve, our instrument can
561 automatically measure up to eight or even more samples in each batch analysis without
562 requiring any operator attention, which could thus save time and labor during analyses. In
563 addition, the advantages of easy handling and high stability indicate the system has the
564 potential to conduct continuous shipboard measurements or be deployed in the field for a
565 relatively long period. However, further testing is needed to confirm the potential of this
566 technique. Using data of DIC and δ^{13}C-DIC from the Chesapeake Bay field survey on 4-6
567 May 2016, we conclude that DIC and its isotopic composition were primarily controlled
568 by carbonate precipitation and CO_2 outgassing in the northern regions of the upper bay,
569 but by primary production and degradation of organic carbon in the southern parts of

upper bay and the middle bay. This application provides new insight for distinguishing the main controls on DIC and δ^{13}C-DIC in estuarine and coastal environments. By improving the mode of sample introduction, the system offers the potential to expand the temporal and spatial coverage of paired DIC and δ^{13}C-DIC, facilitating future research into complex carbonate system questions across a wide range of aquatic settings.

Acknowledgements

We thank Neil C. Sturchio and Linnea Heraty for verifying the δ^{13}C values of $NaHCO_3$ solids on IRMS. We thank the engineers at the Apollo SciTech for system design, hardware and software. We thank Sarah Cooley for assistance with English. The fieldwork was supported by a NOAA grant NA15NOS4780190. During the period of data synthesis and manuscript writing, support by a Delaware Bioscience Center for Advanced Technology (CAT) Applied Research Collaborations (ARC) award is acknowledged. We thank three anonymous reviewers for their insightful and constructive comments.

References

Alling, V., Porcelli, D., Mörth, C.M., Anderson, L.G., Sanchez-Garcia, L., Gustafsson, Ö., Andersson, P.S. and Humborg, C., 2012. Degradation of terrestrial organic carbon, primary production and out-gassing of CO_2 in the Laptev and East Siberian Seas as inferred from δ^{13}C values of DIC. Geochim. Cosmochim. Acta, 95: 143-159.

Amornthammarong, N., Ortner, P.B., Hendee, J. and Woosley, R., 2014. A simplified coulometric method for multi-sample measurements of total dissolved inorganic carbon concentration in marine waters. Analyst, 139(20): 5263-5270.

Becker, M., Andersen, N., Fiedler, B., Fietzek, P., Körtzinger, A., Steinhoff, T. and Friedrichs, G., 2012. Using cavity ringdown spectroscopy for continuous

monitoring of $\delta^{13}C(CO_2)$ and fCO_2 in the surface ocean. Limnol. Oceanogr. Methods, 10(10): 752-766.

Becker, M., Andersen, N., Erlenkeuser, H., Humphreys, M.P., Toste, T. and Körtzinger, A., 2016. An internally consistent dataset of $\delta^{13}C$-DIC in the North Atlantic Ocean - NAC13v1. Earth Syst. Sci. Data, 8(2): 559-570.

Bergamaschi, P., Schupp, M. and Harris, G.W., 1994. High-precision direct measurements of $^{13}CH_4/^{12}CH_4$ and $^{12}CH_3D/^{12}CH_4$ ratios in atmospheric methane sources by means of a long-path tunable diode laser absorption spectrometer. Appl. Opt., 33(33): 7704-7716.

Bianchi, T.S., 2011. The role of terrestrially derived organic carbon in the coastal ocean: A changing paradigm and the priming effect. Proc. Natl. Acad. Sci. U.S.A., 108(49): 19473-19481.

Boicourt, W.C., Kuzmić, M. and Hopkins, T.S., 1999. The inland sea: circulation of Chesapeake Bay and the Northern Adriatic. In: Malone, T.C., Malej, A., Harding Jr, L.W., Smodlaka, N. and Turner, R.E. (Eds.), Ecosystems at the land-sea margin: drainage basin to coastal sea. American Geophysical Union, Washington, DC, pp. 81-129.

Cai, W.-J., Huang, W.-J., Luther, G.W., Pierrot, D., Li, M., Testa, J., Xue, M., Joesoef, A., Mann, R., Brodeur, J., Xu, Y.-Y., Chen, B., Hussain, N., Waldbusser, G.G., Cornwell, J. and Kemp, W.M., 2017. Redox reactions and weak buffering capacity lead to acidification in the Chesapeake Bay. Nat. Commun., 8: 369.

Call, M., Schulz, K.G., Carvalho, M.C., Santos, I.R. and Maher, D.T., 2017. Technical note: Coupling infrared gas analysis and cavity ring down spectroscopy for autonomous, high-temporal-resolution measurements of DIC and $\delta^{13}C$–DIC. Biogeosciences, 14(5): 1305-1313.

Cardenas-Valencia, A.M., Adornato, L.R., Bell, R.J., Byrne, R.H. and Short, R.T., 2013. Evaluation of reagentless pH modification for in situ ocean analysis: determination of dissolved inorganic carbon using mass spectrometry. Rapid Commun. Mass Spectrom., 27(5): 635-642.

Cheng, L., Normandeau, C., Bowden, R., Doucett, R., Gallagher, B., Gillikin, D.P., Kumamoto, Y., McKay, J.L., Middlestead, P., Ninnemann, U., Nothaft, D., Dubinina, E.O., Quay, P., Reverdin, G., Shirai, K., Mørkved, P.T., Theiling, B.P., van Geldern, R. and Wallace, D.W.R., 2019. An international intercomparison of stable carbon isotope composition measurements of dissolved inorganic carbon in seawater. Limnol. Oceanogr. Methods.

Coplen, T.B., Brand, W.A., Gehre, M., Gröning, M., Meijer, H.A.J., Toman, B. and Verkouteren, R.M., 2006. New Guidelines for $\delta^{13}C$ Measurements. Anal. Chem., 78(7): 2439-2441.

Crosson, E.R., 2008. A cavity ring-down analyzer for measuring atmospheric levels of methane, carbon dioxide, and water vapor. Appl. Phys. B, 92(3): 403-408.

Dickson, A.G., Sabine, C.L. and Christian, J.R. (Eds.), 2007. Guide to best practices for ocean CO_2 measurements. PICES Special Publication 3, 191 pp.

Du, J. and Shen, J., 2016. Water residence time in Chesapeake Bay for 1980–2012. J. Mar. Syst., 164: 101-111.

Friederich, G.E., Walz, P.M., Burczynski, M.G. and Chavez, F.P., 2002. Inorganic carbon in the central California upwelling system during the 1997–1999 El Niño–La Niña event. Prog. Oceanogr., 54(1): 185-203.

Friedrichs, G., Bock, J., Temps, F., Fietzek, P., Körtzinger, A. and Wallace, D.W.R., 2010. Toward continuous monitoring of seawater $^{13}CO_2/^{12}CO_2$ isotope ratio and pCO_2: Performance of cavity ringdown spectroscopy and gas matrix effects. Limnol. Oceanogr. Methods, 8(10): 539-551.

Gruber, N., Keeling, C.D., Bacastow, R.B., Guenther, P.R., Lueker, T.J., Wahlen, M., Meijer, H.A.J., Mook, W.G. and Stocker, T.F., 1999. Spatiotemporal patterns of carbon-13 in the global surface oceans and the oceanic suess effect. Global Biogeochem. Cycles, 13(2): 307-335.

Hagy, J.D., Boynton, W.R., Keefe, C.W. and Wood, K.V., 2004. Hypoxia in Chesapeake Bay, 1950–2001: Long-term change in relation to nutrient loading and river flow. Estuaries, 27(4): 634-658.

Han, A., Dai, M., Kao, S.-J., Gan, J., Li, Q., Wang, L., Zhai, W. and Wang, L., 2012. Nutrient dynamics and biological consumption in a large continental shelf system under the influence of both a river plume and coastal upwelling. Limnol. Oceanogr., 57(2): 486-502.

Hellings, L., Dehairs, F., Tackx, M., Keppens, E. and Baeyens, W., 1999. Origin and fate of organic carbon in the freshwater part of the Scheldt Estuary as traced by stable carbon isotope composition. Biogeochemistry, 47(2): 167-186.

Hu, X., Cai, W.-J., Rabalais, N.N. and Xue, J., 2016. Coupled oxygen and dissolved inorganic carbon dynamics in coastal ocean and its use as a potential indicator for detecting water column oil degradation. Deep Sea Res. Part II Top. Stud. Oceanogr., 129: 311-318.

Huang, K., Cassar, N., Wanninkhof, R. and Bender, M., 2013. An isotope dilution method for high-frequency measurements of dissolved inorganic carbon concentration in the surface ocean. Limnol. Oceanogr. Methods, 11: 572-583.

Huang, K., Cassar, N., Jonsson, B., Cai, W.-j. and Bender, M.L., 2015. An Ultrahigh Precision, High-Frequency Dissolved Inorganic Carbon Analyzer Based on Dual Isotope Dilution and Cavity Ring-Down Spectroscopy. Environ. Sci. Technol., 49(14): 8602-8610.

Huang, W.J., Wang, Y. and Cai, W.J., 2012. Assessment of sample storage techniques for total alkalinity and dissolved inorganic carbon in seawater. Limnol. Oceanogr. Methods, 10(9): 711-717.

Humphreys, M.P., Achterberg, E.P., Griffiths, A.M., McDonald, A. and Boyce, A.J., 2015. Measurements of the stable carbon isotope composition of dissolved inorganic carbon in the northeastern Atlantic and Nordic Seas during summer 2012. Earth Syst. Sci. Data, 7(1): 127-135.

Jäger, F., Wagner, G., Meijer, H.A.J. and Kerstel, E.R.T., 2005. Measuring $\delta^{13}C$ of atmospheric air with non-dispersive infrared spectroscopy. Isotopes Environ. Health Stud., 41(4): 373-378.

Jost, H.-J., Castrillo, A. and Wilson, H.W., 2006. Simultaneous $^{13}C/^{12}C$ and $^{18}O/^{16}O$ isotope ratio measurements on CO_2 based on off-axis integrated cavity output spectroscopy. Isotopes Environ. Health Stud., 42(1): 37-45.

686 Kemp, W., Boynton, W., Adolf, J., Boesch, D., Boicourt, W., Brush, G., Cornwell, J.,
687 Fisher, T., Glibert, P. and Hagy, J., 2005. Eutrophication of Chesapeake Bay:
688 historical trends and ecological interactions. Mar. Ecol. Prog. Ser., 303(21): 1-29.
689 Kemp, W.M., Smith, E.M., Marvin-DiPasquale, M. and Boynton, W.R., 1997. Organic
690 carbon balance and net ecosystem metabolism in Chesapeake Bay. Mar. Ecol.
691 Prog. Ser., 150(1/3): 229-248.
692 Mohn, J., Werner, R.A., Buchmann, B. and Emmenegger, L., 2007. High-precision
693 $\delta^{13}CO_2$ analysis by FTIR spectroscopy using a novel calibration strategy. J. Mol.
694 Struct., 834-836: 95-101.
695 Murphy, R.R., Kemp, W.M. and Ball, W.P., 2011. Long-Term Trends in Chesapeake Bay
696 Seasonal Hypoxia, Stratification, and Nutrient Loading. Estuar. Coast., 34(6):
697 1293-1309.
698 Nara, H., Tanimoto, H., Tohjima, Y., Mukai, H., Nojiri, Y., Katsumata, K. and Rella, C.,
699 2012. Effect of air composition (N_2, O_2, Ar, and H_2O) on CO_2 and CH_4
700 measurement by wavelength-scanned cavity ring-down spectroscopy: calibration
701 and measurement strategy. Atmos. Meas. Tech., 5(11): 2689.
702 O'Sullivan, D.W. and Millero, F.J., 1998. Continual measurement of the total inorganic
703 carbon in surface seawater. Mar. Chem., 60(1): 75-83.
704 Paul, D., Skrzypek, G. and Fórizs, I., 2007. Normalization of measured stable isotopic
705 compositions to isotope reference scales – a review. Rapid Commun. Mass
706 Spectrom., 21(18): 3006-3014.
707 Quay, P., Sonnerup, R., Westby, T., Stutsman, J. and McNichol, A., 2003. Changes in the
708 $^{13}C/^{12}C$ of dissolved inorganic carbon in the ocean as a tracer of anthropogenic
709 CO_2 uptake. Global Biogeochem. Cycles, 17(1): 4-1-4-20.
710 Rau, G.H., Riebesell, U. and Wolf-Gladrow, D., 1996. A model of photosynthetic ^{13}C
711 fractionation by marine phytoplankton based on diffusive molecular CO_2 uptake.
712 Mar. Ecol. Prog. Ser., 133: 275-285.
713 Samanta, S., Dalai, T.K., Pattanaik, J.K., Rai, S.K. and Mazumdar, A., 2015. Dissolved
714 inorganic carbon (DIC) and its $\delta^{13}C$ in the Ganga (Hooghly) River estuary, India:
715 Evidence of DIC generation via organic carbon degradation and carbonate
716 dissolution. Geochim. Cosmochim. Acta, 165: 226-248.
717 Schubel, J. and Pritchard, D., 1986. Responses of upper Chesapeake Bay to variations in
718 discharge of the Susquehanna River. Estuaries, 9(4): 236-249.
719 Smith, E.M. and Kemp, W.M., 1995. Seasonal and regional variations in plankton
720 community production and respiration for Chesapeake Bay. Mar. Ecol. Prog. Ser.,
721 116(1): 217-231.
722 Su, J., Dai, M., He, B., Wang, L., Gan, J., Guo, X., Zhao, H. and Yu, F., 2017. Tracing
723 the origin of the oxygen-consuming organic matter in the hypoxic zone in a large
724 eutrophic estuary: the lower reach of the Pearl River Estuary, China.
725 Biogeosciences, 14(18): 4085-4099.
726 Taylor, J.R., 1997. Introduction to error analysis, the Study of Uncertainties in Physical
727 Measurements, 2nd Edition. University Science Books, New York.
728 van Geldern, R., Verma, M.P., Carvalho, M.C., Grassa, F., Delgado-Huertas, A.,
729 Monvoisin, G. and Barth, J.A.C., 2013. Stable carbon isotope analysis of
730 dissolved inorganic carbon (DIC) and dissolved organic carbon (DOC) in natural

waters – Results from a worldwide proficiency test. Rapid Commun. Mass Spectrom., 27(18): 2099-2107.

Wahl, E.H., Fidric, B., Rella, C.W., Koulikov, S., Kharlamov, B., Tan, S., Kachanov, A.A., Richman, B.A., Crosson, E.R., Paldus, B.A., Kalaskar, S. and Bowling, D.R., 2006. Applications of cavity ring-down spectroscopy to high precision isotope ratio measurement of $^{13}C/^{12}C$ in carbon dioxide. Isotopes Environ. Health Stud., 42(1): 21-35.

Wang, H., Dai, M., Liu, J., Kao, S.-J., Zhang, C., Cai, W.-J., Wang, G., Qian, W., Zhao, M. and Sun, Z., 2016. Eutrophication-Driven Hypoxia in the East China Sea off the Changjiang Estuary. Environ. Sci. Technol., 50: 2255-2263.

Wang, Z.A., Liu, X., Byrne, R.H., Wanninkhof, R., Bernstein, R.E., Kaltenbacher, E.A. and Patten, J., 2007. Simultaneous spectrophotometric flow-through measurements of pH, carbon dioxide fugacity, and total inorganic carbon in seawater. Anal. Chim. Acta, 596(1): 23-36.

Yang, X., Xue, L., Li, Y., Han, P., Liu, X., Zhang, L. and Cai, W.-J., 2018. Treated Wastewater Changes the Export of Dissolved Inorganic Carbon and Its Isotopic Composition and Leads to Acidification in Coastal Oceans. Environ. Sci. Technol., 52(10): 5590-5599.

Zeebe, R.E. and Wolf-Gladrow, D.A., 2001. CO_2 in seawater: equilibrium, kinetics, isotopes. Elsevier, Amsterdam.

764 Table 1. Summary of endmember values and their uncertainties.

Endmembers	Salinity (psu)	DIC ($\mu mol\ kg^{-1}$)	$\delta^{13}C$-DIC (‰)
Riverine	0	1091.7±73.6	-7.3±0.2[a]
Offshore	33.618±0.139[b]	2063.5±11.0	1.3±0.1[c]

765 [a]Average value of $\delta^{13}C$-DIC in the Susquehanna River in the spring and summer of 2006
766 in Hossler and Bauer (2012).
767 [b]The salinity of the ocean endmember in Cai et al. (2017).
768 [c]Cited from Quay et al. (2007) according to the latitude range of the Chesapeake Bay (36-
769 40 °N).
770
771

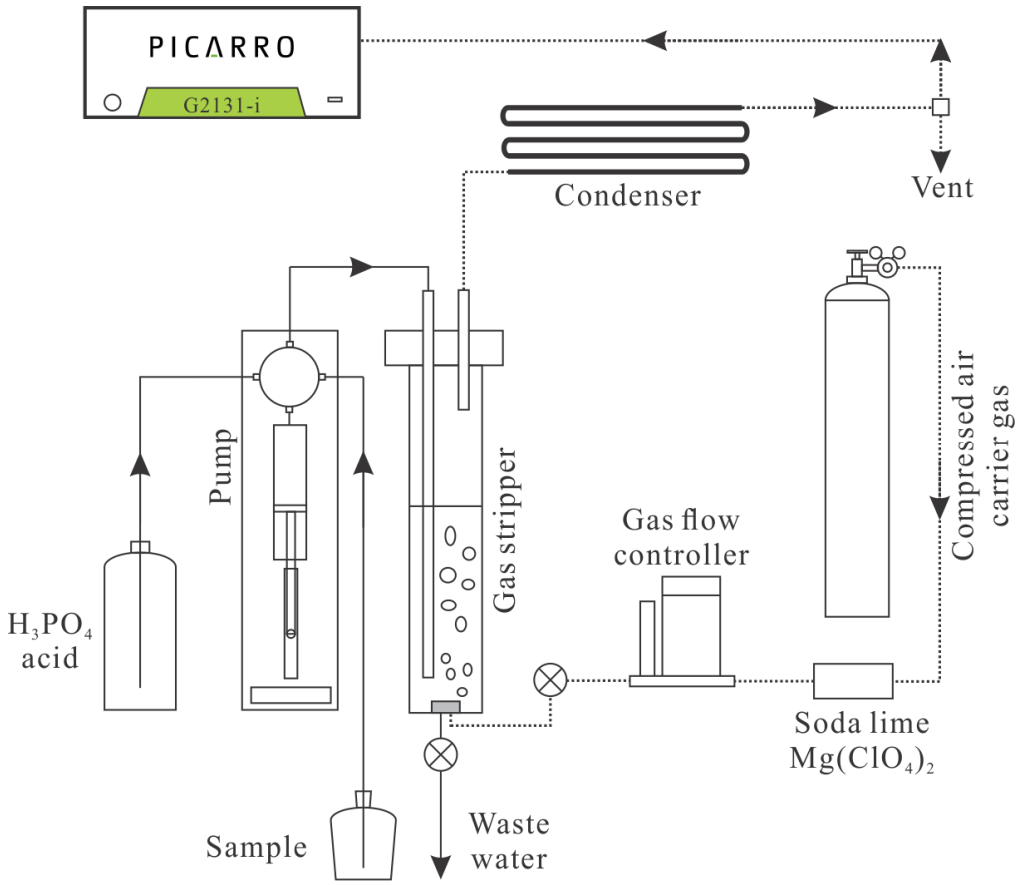

772

773 Fig. 1. A simplified schematic setup of the coupled CO_2 extraction device and Cavity

774 Ring-Down Spectrometer (CRDS) to simultaneously measure DIC and δ^{13}C-DIC. Note

775 that the solid arrows mean liquid flow, while the dashed arrows mean gas flow. A

776 photograph of the system can be found at the manufacturer's webpage

777 (www.apolloscitech.com).

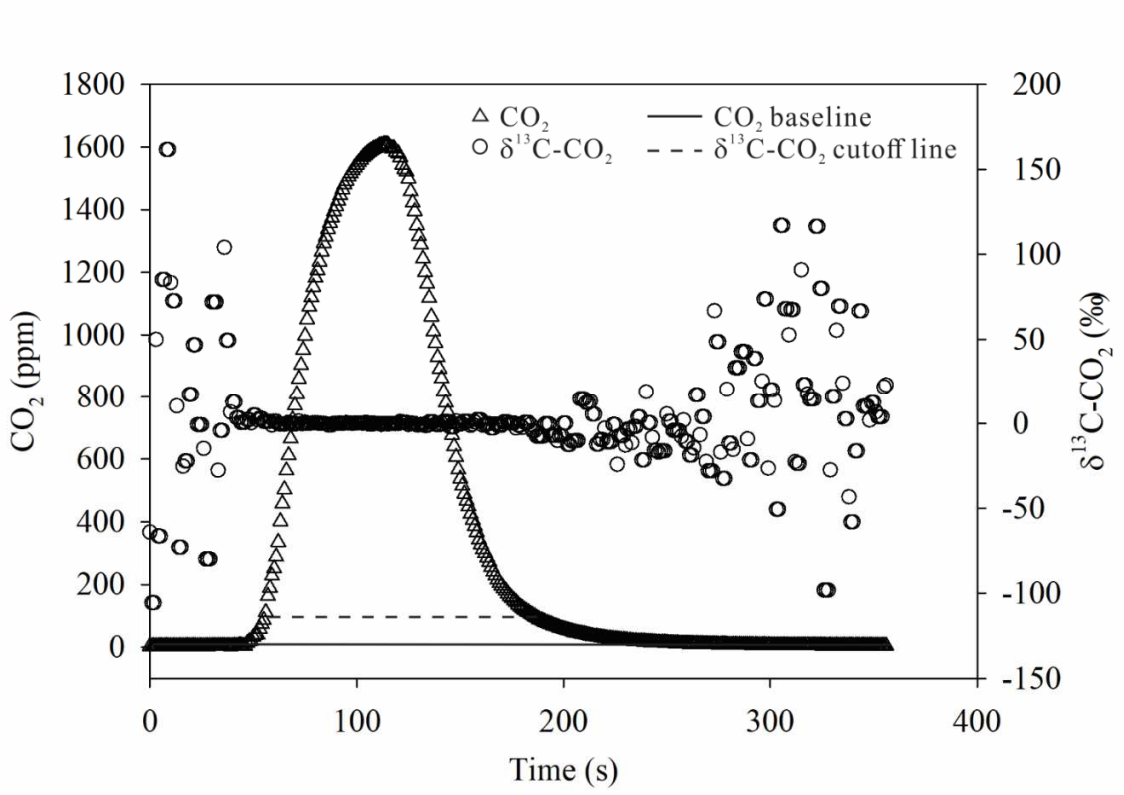

778

779 Fig. 2. Typical output from the CRDS showing data collected for one measurement for

780 CO_2 (triangles) and $\delta^{13}C$-CO_2 (circles). Net integration area for DIC is obtained by

781 integrating the area under the curve marked with triangles over the solid baseline. The

782 $\delta^{13}C$-DIC is derived from the integrated area above the dashed line and beneath the

783 triangle curve and the corresponding $\delta^{13}C$-CO_2 values.

784

785

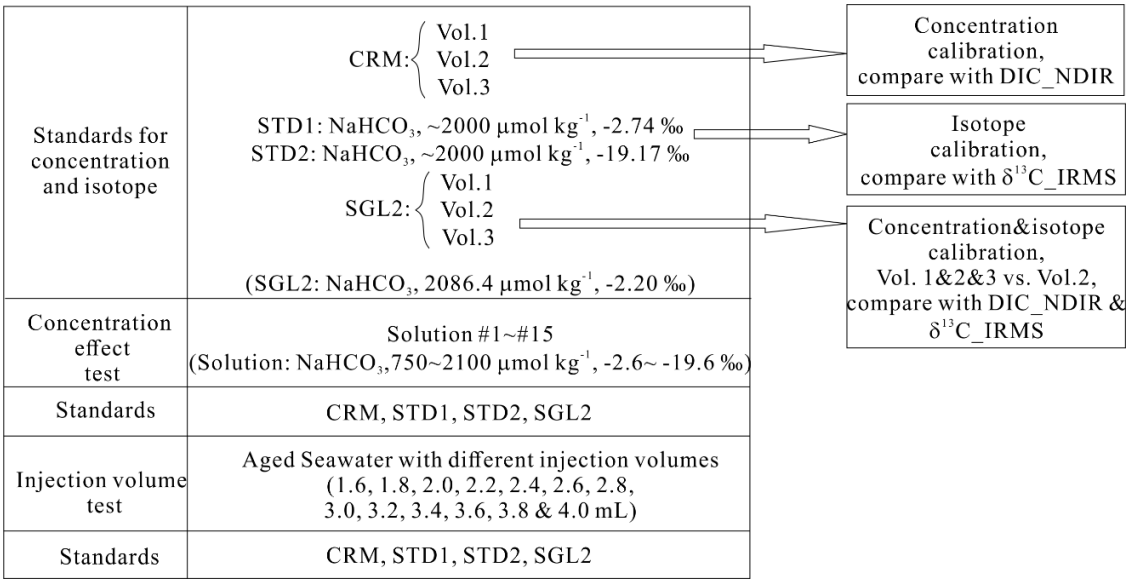

786

787 Fig. 3. Schematic showing evaluation of system performance.

788

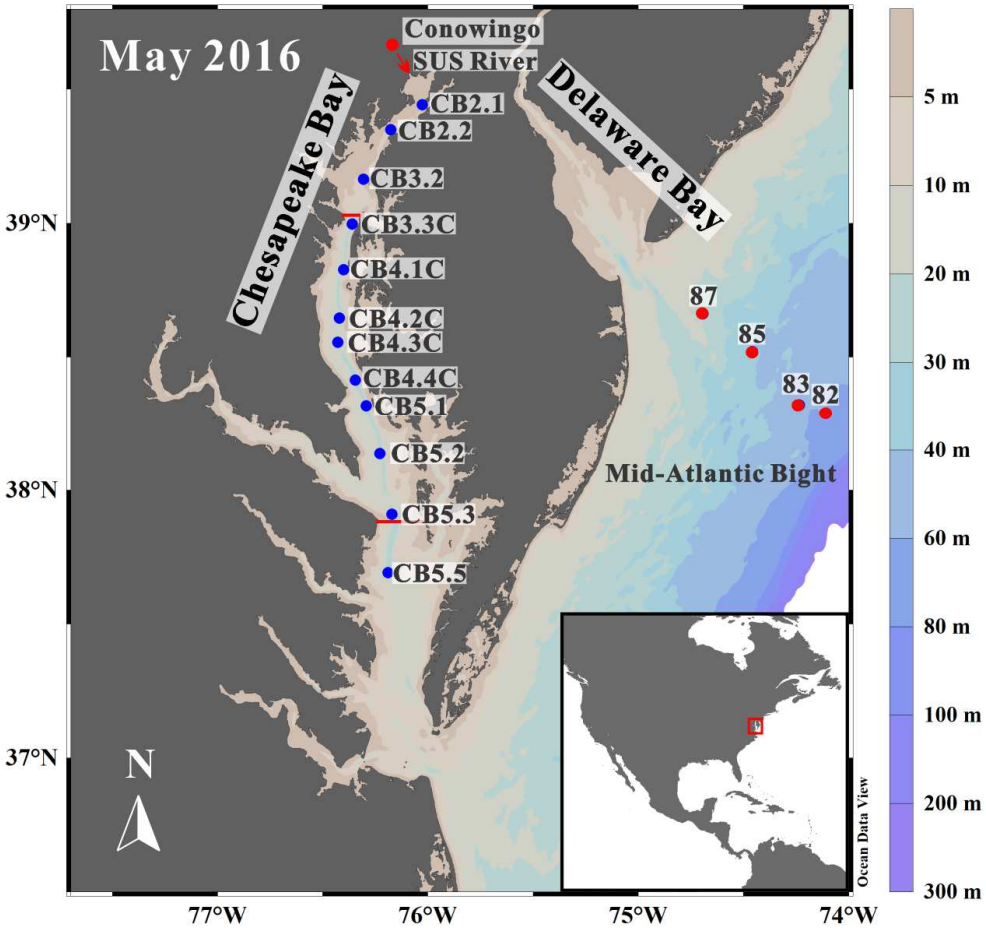

789

790 Fig. 4. Sampling stations (blue) in the Chesapeake Bay in May 2016. Red circles
791 represent the river endmember at Conowingo in the Susquehanna River, and offshore
792 seawater endmember at four stations in the Mid-Atlantic Bight. The arrow points to the
793 outlet of the Susquehanna River. The red lines divide the main channel into three sub-
794 regions, i.e., upper bay (39.0-39.5° N), middle bay (37.9-39.0° N) and lower bay (37.0-
795 37.9° N). The inserted regional map indicates the location of the Chesapeake Bay.

796

797

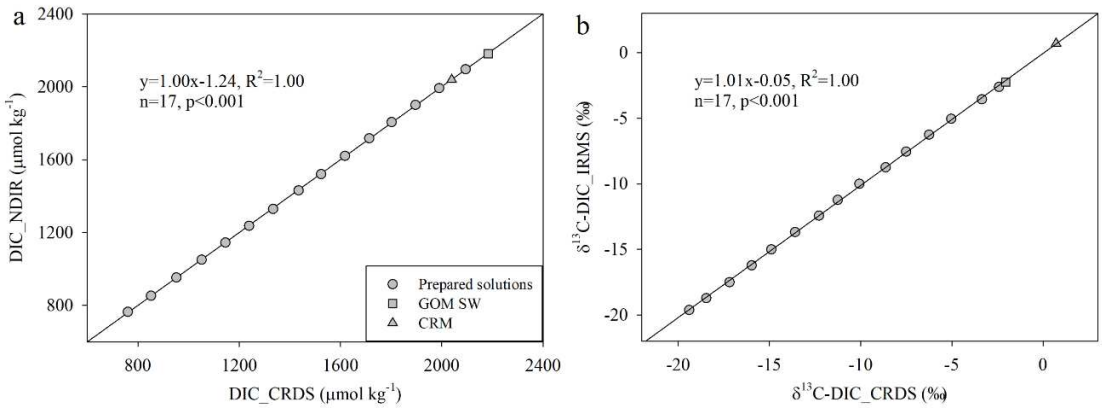

798

799 Fig. 5. Intercomparison of DIC between CRDS and NDIR (a), and δ^{13}C-DIC between

800 CRDS and IRMS (b). Slope of ~1.00 shows excellent agreement not only between two

801 different methodologies, but also laboratories.

802

803

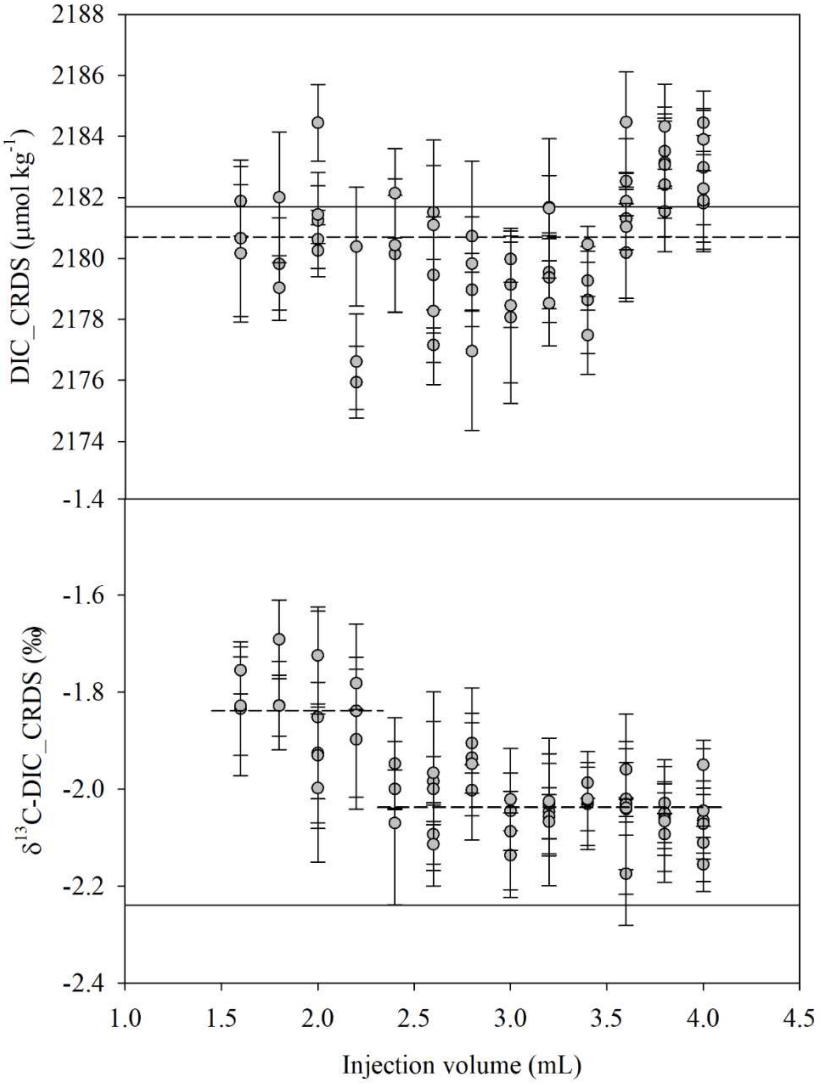

Fig. 6. The measured DIC and δ^{13}C-DIC of aged Gulf of Mexico seawater with different injection volumes. In the upper panel, the dashed line represents the average of measured DIC values from CRDS, while the solid reference line indicates the average DIC value from NDIR. In the lower panel, the dashed lines show the average δ^{13}C-DIC values from CRDS in two separate injection volume ranges. The solid reference line indicates the δ^{13}C-DIC value certified by IRMS.

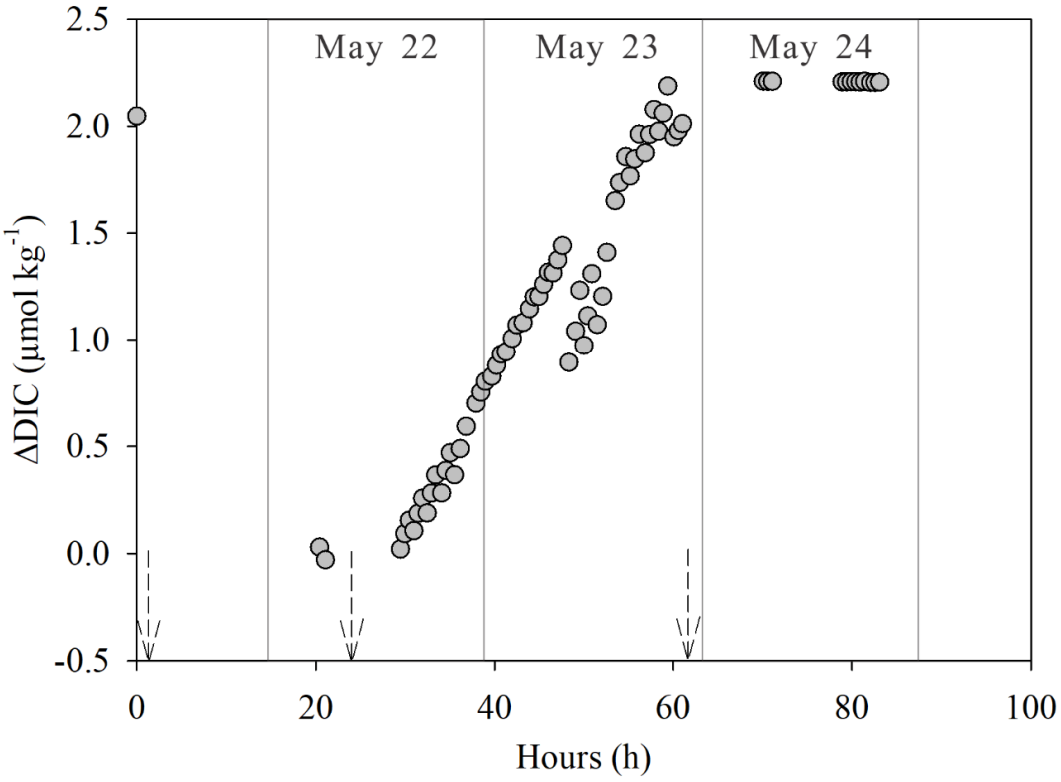

Fig. 7. Differences in DIC relative to the time of measurement. Seawater from the Gulf of Mexico was used in these analyses to check the instrument drift over time. Differences in DIC values were estimated by (i) using the calibration curve of the 1st day (May 22) and (ii) the calibration curves of each individual day (May 22-24). The three dashed arrows indicate times when standards were run. Note that the dot in May 21 is a warm up test before carrying out the standard measurement.

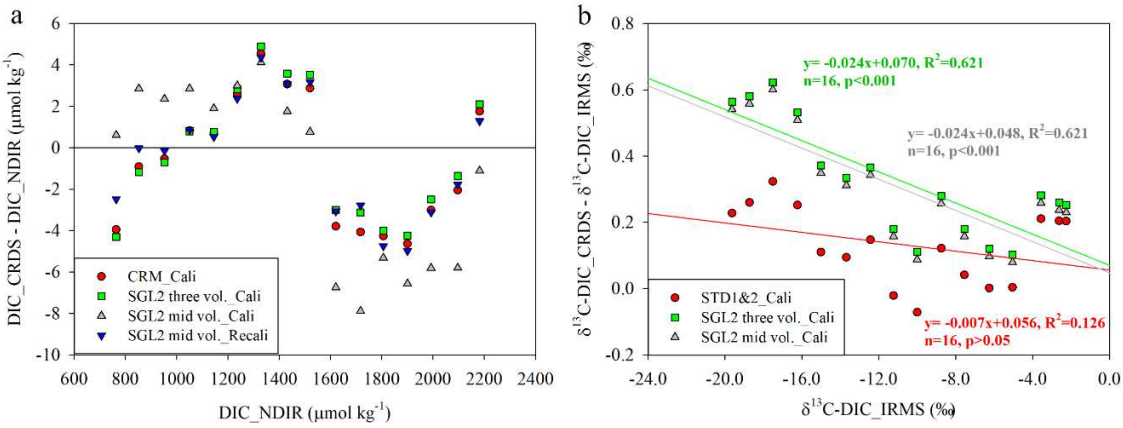

Fig. 8. Comparison of the offset values (i.e., DIC_CRDS - DIC_NDIR and δ^{13}C-DIC_CRDS - δ^{13}C-DIC_IRMS) using different calibration methods. (a) For DIC, three volumes of CRM (red), three volumes of SGL2 (green) and a middle volume of SGL2 (grey) were used to calibrate the output data. The results of the middle volume SGL2 calibration (blue) were further recalibrated so as to remove the systematic error from single-point calibration. (b) For δ^{13}C-DIC, one volume of STD1 (-2.74±0.10 ‰) and STD2 (-19.17±0.10 ‰) each (red), three volumes of SGL2 (-2.20±0.10 ‰) (green) and a middle volume of SGL2 (grey) were used to calibrate the output data.

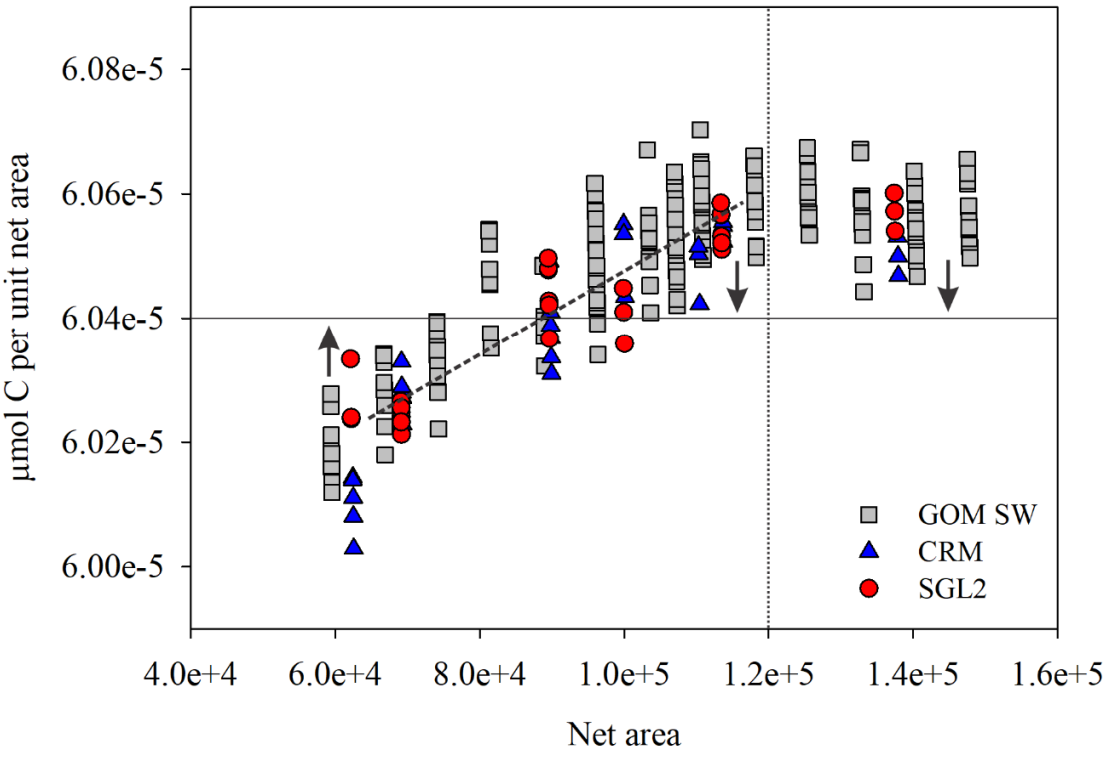

833

834 Fig. 9. The relationship between DIC content (µmol C) of unit net area and net area. The
835 vertical dotted line is a reference line separating an increasing zone in the left and a
836 constant zone in the right. The horizontal solid line indicates the average value (6.04×10^{-5}
837 µmol C per unit net area) of the middle volume of SGL2 analyzed, which was adopted in
838 the third method of DIC calibration (see text). The systematic errors affecting the third
839 method are denoted by arrows, where an upward arrow indicates an overestimate and a
840 downward arrow indicates an underestimate. The dashed line represents the linear
841 regression line of three volumes (2.0, 2.6, and 3.3 mL) of SGL2 with R^2=0.89.

842

843

844

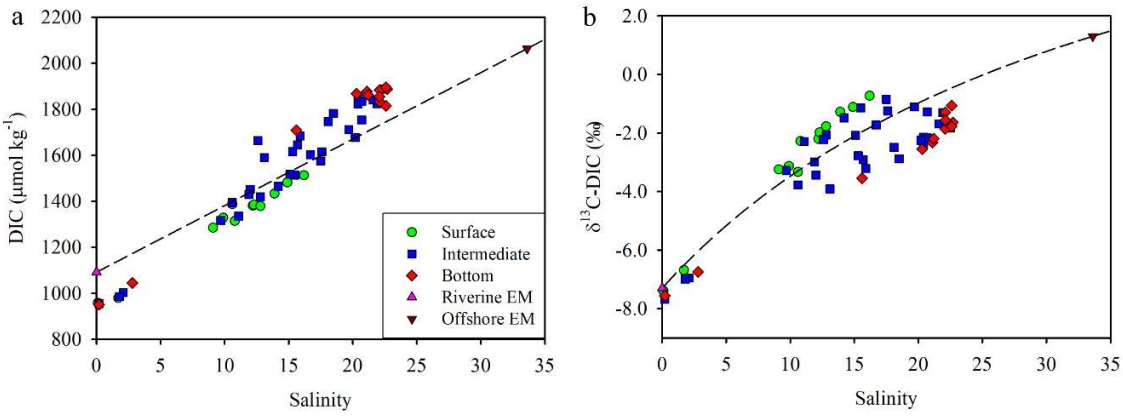

845

846 Fig. 10. Distributions of DIC and δ^{13}C-DIC against salinity in the Chesapeake Bay in

847 May 2016. The dashed lines indicate conservative mixing between Susquehanna River

848 water and offshore seawater in the Mid-Atlantic Bight.

849

850

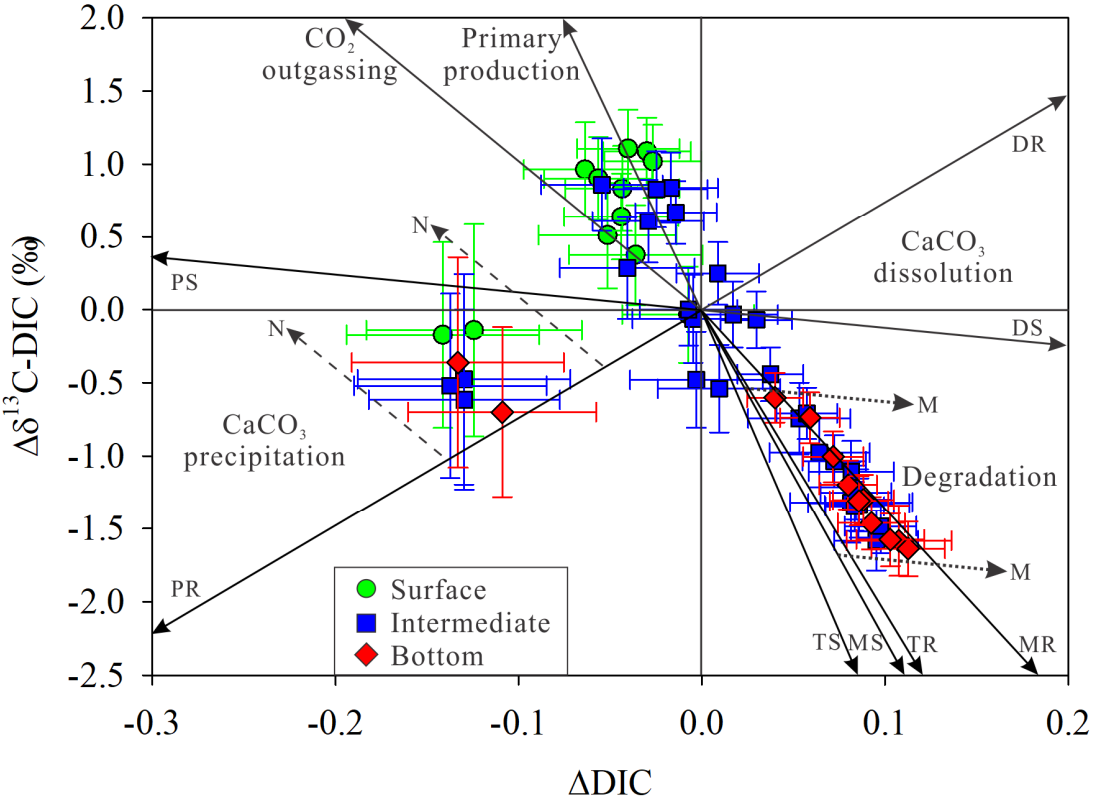

851

852 Fig. 11. The deviations of DIC concentrations (ΔDIC) and δ^{13}C-DIC ($\Delta\delta^{13}$C-DIC)
853 relative to the conservative mixing line in the Chesapeake Bay in May 2016. Note that
854 the origin represents the data only controlled by conservative mixing. The data points
855 would deviate from the origin in directions shown with solid vectors if they were
856 influenced by a specific additional process, or shown with dashed and dotted vectors if
857 they were influenced by more than one process. See main text for details on drawing
858 these vectors. The four vectors (TS, TR, MS, MR) represent effects of degradation of
859 organic carbon, which depend on the sources of organic carbon (T: terrestrial source; M:
860 marine source) and the initial DIC and δ^{13}C-DIC composition in the water (S: seawater;
861 R: river water). Vectors DS and DR, drawn using the δ^{13}C-DIC of seawater and river

862 water, respectively, denote the effect of $CaCO_3$ dissolution. Similarly, vectors PS and PR
863 indicate the effect of $CaCO_3$ precipitation. Vectors in the upper left quadrant indicate the
864 effects of primary production or CO_2 outgassing. Dashed vectors marked N, which are
865 drawn parallel to vector CO_2 outgassing, indicate the effect of $CaCO_3$ precipitation
866 followed by CO_2 outgassing. Dotted vectors marked M, which are drawn parallel to
867 vector DS, illustrate the effect of degradation of organic carbon followed by $CaCO_3$
868 dissolution.